Diffusive Shock Acceleration and Turbulent Reconnection

Christian Garrel, Loukas Vlahos, Heinz Isliker, Theophilos Pisokas

Monthly Notices
of the
ROYAL ASTRONOMICAL SOCIETY

MNRAS **478,** 2976–2986 (2018)
Advance Access publication 2018 May 15

doi:10.1093/mnras/sty1260

Diffusive shock acceleration and turbulent reconnection

Christian Garrel,[1,2] Loukas Vlahos,[2]★ Heinz Isliker[2] and Theophilos Pisokas[2]

[1]*Département de Physique de l' Université de Nice Sophia-Antipolis and Observatoire de la Côte d' Azur, Université Côte d' Azur (MAUCA), Parc Valrose, F-06100 Nice, France*
[2]*Department of Physics, Aristotle University, 54124 Thessaloniki, Greece*

Accepted 2018 May 13. Received 2018 March 27; in original form 2018 February 4

ABSTRACT

Diffusive shock acceleration (DSA) cannot efficiently accelerate particles without the presence of self-consistently generated or pre-existing strong turbulence ($\delta B/B\sim 1$) in the vicinity of the shock. The problem we address in this article is: if large-amplitude magnetic disturbances are present upstream and downstream of a shock then Turbulent Reconnection (TR) will set in and will participate not only in the elastic scattering of particles but also in their heating and acceleration. We demonstrate that large-amplitude magnetic disturbances and Unstable Current Sheets (UCS), spontaneously formed in the strong turbulence in the vicinity of a shock, can accelerate particles as efficiently as DSA in *large-scale systems and on long time scales*. We start our analysis with 'elastic' scatterers upstream and downstream and estimate the energy distribution of particles escaping from the shock, recovering the well-known results from the DSA theory. Next we analyse the additional interaction of the particles with active scatterers (magnetic disturbances and UCS) upstream and downstream of the shock. We show that the asymptotic energy distribution of the particles accelerated by DSA/TR has very similar characteristics with the one due to DSA alone, but the synergy of DSA with TR is much more efficient: The acceleration time is an order of magnitude shorter and the maximum energy reached two orders of magnitude higher. We claim that DSA is the dominant acceleration mechanism in a short period before TR is established, and then strong turbulence will dominate the heating and acceleration of the particles. In other words, the shock serves as the mechanism to set up a strongly turbulent environment, in which the acceleration mechanism will ultimately be the synergy of DSA and TR.

Key words: turbulence – magnetic reconnection.

1 INTRODUCTION

The acceleration of charged particles in space and astrophysical plasmas remains an open problem. In space plasmas the major breakthrough in understanding particle acceleration was made in the beginning of the 50s by Fermi (Fermi 1949, 1954). Fermi proposed two acceleration mechanisms for astrophysical plasmas. One was based on the *stochastic* interaction of particles with large-amplitude magnetic irregularities ('magnetic clouds') and the second one on the *systematic or regular* acceleration of particles by converging magnetic traps.

The studies following the initial ideas proposed by Fermi gradually departed from the concepts put forward by Fermi. The stochastic acceleration (second-order Fermi acceleration) was modelled in the form of resonant or non-resonant interaction of particle with a spectrum of low-amplitude ($\delta B/B << 1$) linear MHD waves (Kulsrud & Ferrari 1971). For more details see the analyses presented in the reviews (Melrose 1994, 2009; Miller, Guessoum & Ramaty 1990; Miller et al. 1997; Petrosian 2012 and the references therein). The systematic acceleration (first-order Fermi acceleration) was modelled as Diffusive Shock acceleration (DSA) (Krymskii 1977; Bell 1978; Blandford & Ostriker 1978; Axford, Leer & Skadron 1978). It is worth discussing briefly the weaknesses of the models used to implement the ideas proposed by Fermi.

The stochastic acceleration or stochastic 'turbulent' acceleration (STA), as it is called, was modelled as the diffusion of particle energy within a spectrum of low-amplitude waves by using the Fokker Planck equation. The transport coefficients were estimated through the quasi-linear approximation (Achterberg 1981). For the STA to be efficient two conditions should be satisfied: (1) The energy of the waves should be sufficiently large and (2) the particles should have a sufficiently large velocity to resonate with the waves (Melrose 1994). The stochastic interaction of particles with low-amplitude waves made this mechanism inefficient for the acceleration of high-energy particles. The strong dependence of the index of the accel-

★ E-mail: vlahos@astro.auth.gr

erated particles on the spectrum of the waves suggested that there is no universal index for the accelerated particles, in contrast to what is usually observed. The STA is not necessarily the correct model for the stochastic acceleration of particles by *large-amplitude* magnetic disturbances, as it has been shown by several authors [see Parker & Tidman 1958; Ramaty 1979; Pisokas et al. 2017]. We believe that the stochastic scattering of electrons and ions off large-amplitude magnetic fluctuation should be based again on the original ideas put forward by Fermi (1949).

The evolution of large-amplitude MHD waves, needed to scatter particles in the vicinity of a shock, is a very interesting problem and has been analysed in several articles (Biskamp & Welter 1989; Dmitruk et al. 2003; Dmitruk, Matthaeus & Seenu 2004; Arzner & Vlahos 2004; Arzner et al. 2006; Servidio et al. 2010, 2011; Isliker, Vlahos & Constantinescu 2017a) and reviews (Matthaeus & Velli 2011; Karimabadi & Lazarian 2013; Karimabadi et al. 2013). All the above studies agree that strong turbulence leads to the spontaneous formation of an environment that we will call here Turbulent Reconnection (TR), and which is dominated by large-amplitude magnetic fluctuations and Unstable Current Sheets (UCS; Matthaeus & Lamkin 1986; Lazarian & Vishniac 1999; Lazarian et al. 2015). The interaction of electrons and ions with plasmas in the TR state has been analysed by Ambrosiano et al. (1988), Dmitruk, Matthaeus & Seenu (2004), Arzner et al. (2006), Vlahos et al. (2016), Pisokas et al. (2017), Isliker et al. (2017b) and Pisokas, Vlahos & Isliker (2018).

The acceleration of particles in the vicinity of a shock is a prominent acceleration mechanism for astrophysical plasmas. The details on how this mechanism will operate in different cosmic environments remain an open and very complex problem [see the reviews Drury (1983); Burgess, Möbius & Scholer (2012); Schure et al. (2012)].

In the heliosphere, the Coronal Mass Ejection (CME) shock, the Earth's and planetary Bow Shocks interact with the Solar Wind, which is already in a TR state (Osman et al. 2014; Zank et al. 2014; Chasapis et al. 2015; Matthaeus et al. 2015; Khabarova et al. 2016; Khabarova & Zank 2017). Downstream of the heliospheric shocks the amplitude of the magnetic fluctuations becomes even stronger and the formation of a TR environment is easier to establish. The presence of a TR environment in the Heliospheric Termination Shock is under intense discussion (Lazarian & Opher 2009; Drake et al. 2010; Burgess, Gingell & Matteini 2016).

The role of Shock acceleration during Supernova Remnants (SNR) and its importance for accelerating cosmic rays is still an open problem in High-Energy Astrophysics. A major concern in the theory of particle acceleration through DSA in SNR is the mechanism which traps the accelerated particles in the vicinity of the shock surface. The large-amplitude magnetic fluctuations upstream and downstream of the shock can be driven by different MHD or kinetic instabilities [see the review of Bykov et al. (2013)]. The interaction of the shock precursor with density fluctuations in the pre-shock media (del Valle et al. 2018) or the post-shock turbulence arising from various instabilities (Balsara, Benjamin & Cox 2001; Balsara, & Kim 2005; Giacalone & Jokipii 2007) can create large-amplitude MHD perturbations. Bell (2004) proposed that turbulence upstream can be excited by current-driven instabilities of accelerated particles. The most advanced recent simulations (Caprioli & Spitkovsky 2014a,b,c; Bai et al. 2015; van Marle, Casse & Marcowith 2018) so far cannot capture the large spatial scales and the long-term evolution of the excited instabilities and interactions involved in realistic astrophysical systems, i.e. their results cover only the microphysics of the very early moments of the shock acceleration.

The link between shock and TR has been analysed by Karimabadi et al. (2014), using large-scale PIC simulations. The presence of reconnecting current sheets in the vicinity of the shock and their role in the acceleration of particles has been analysed also in depth by several authors (see Zank et al. 2015; Matsumoto et al. 2015; le Roux et al. 2016). The importance of TR in the vicinity of the shock and its role in heating and accelerating particles is currently a very important problem waiting its solution.

In this article we start by analyzing DSA, assuming scatterers upstream and downstream that are elastic. We then move on to study the role of stochastic acceleration in DSA by assuming that the scatters are active, mostly in the form of large-amplitude magnetic fluctuations. In the final step we assume that a percentage of the scatterers are UCS, modelling a TR state of the plasma in the vicinity of the shock. In the current literature the case of DSA in the presence of UCS has been studied (Zank et al. 2015; le Roux et al. 2016), as well as the acceleration of particles by TR in the absence of a shock (Pisokas et al. 2018).

The structure of our article is as follows: in Section 2 we review briefly the basic theoretical results of DSA, and in Section 3 we propose a large-scale model for DSA. In Section 4.1 we present our results for passive scatterers, and in Sections 4.2 and 4.3 for active scatterers, assuming that their interaction is either stochastic or stochastic and systematic.

2 DIFFUSIVE SHOCK ACCELERATION

DSA is based on the assumption that particles can be confined near the shock discontinuity by scattering off Magnetohydrodyanmic large-scale disturbances that act as scattering centres. The scattering mean-free path λ_{sc} is assumed to be much larger than the shock thickness and much shorter than the length L of the area where the wave activity upstream and downstream is strong. As a result particles can cross the shock discontinuity repeatedly. The charged particles gain energy through the repeated scatterings off the converging up- and downstream scattering centers.

We define the shock compression ratio as

$$r = \frac{\rho_1}{\rho_2} = \frac{U_1}{U_2} \tag{1}$$

where ρ_1, U_1 are the density and the fluid velocity upstream of the shock, and ρ_2, U_2 the ones downstream. The energy spectrum of the particles accelerated by the shock reaches asymptotically the distribution (Drury 1983)

$$f(p) \sim p^{-3U_1/(U_1-U_2)} \sim p^{-3r/(r-1)}, \tag{2}$$

where p is the momentum of the particles. For strong shocks the compression ratio is $r \sim 4$ and $3r/(r-1) \sim 4$. The fact that the exponent depends only on the compression ratio and reaches asymptotically the value of 4 explains the attractiveness of DSA for astrophysical plasmas.

The analysis of the energy gain $\langle \Delta W \rangle$ of test particles crossing the shock discontinuity yields (see Longair 2011)

$$\frac{\langle \Delta W \rangle}{W} \sim \frac{Uu}{2c^2} \tag{3}$$

where U is the shock velocity, u the velocity of the particle and W the total energy of the particle. From the downstream region the particle can recross the shock, gaining another increment in energy

$(Uu/2c^2)$. The total energy increase for a particle making one round trip is therefore on average

$$\frac{\langle \Delta W \rangle}{W} \sim \frac{Uu}{c^2}. \tag{4}$$

In the downstream region, the scattering process ensures that the particle distribution is isotropic, but occasionally, the flow can sweep particles away from the shock. Particles can thus escape from the downstream area with a finite probability $P_{\rm esc}$. This probability can be calculated as (see Achterberg 2008)

$$P_{\rm esc} \approx \frac{U}{c}. \tag{5}$$

We can now introduce $t_{\rm up}$, $t_{\rm dwn}$ and $t_{\rm cycle}$, respectively, as the times a particle spends on average in the upstream and the downstream region, and the time of a cycle of one round trip across the shock Drury (1983)

$$t_{\rm up} \sim \frac{\lambda_{\rm sc_{up}}}{U} \tag{6}$$

$$t_{\rm dwn} \sim \frac{\lambda_{\rm sc_{dwn}}}{U/4} \tag{7}$$

$$t_{\rm cycle} = t_{\rm up} + t_{\rm dwn} \sim \left(\frac{\lambda_{\rm sc_{up}}}{U} + \frac{\lambda_{\rm sc_{dwn}}}{U/4} \right) \sim \frac{\lambda_{\rm sc_{up}}}{U} \tag{8}$$

(ignoring factors of 2). Assuming that the particles execute a random walk upstream and downstream along their path between the scatterers, the mean square displacement is given as

$$< R^2 >= 6 D_{\rm up/dwn} t \tag{9}$$

where $D_{\rm up/dwn}$ is the diffusion coefficient upstream and downstream, respectively. We can estimate the relation of the mean-free path to the diffusion coefficient for relativistic particles if we assume that $t \sim \lambda_{sc_{\rm up/dwn}}/c$

$$\lambda_{\rm sc_{up}} \sim \frac{D_{\rm up}}{c}, \quad \lambda_{\rm sc_{dwn}} \sim \frac{D_{\rm dwn}}{c}. \tag{10}$$

We notice that we can also re-write $t_{\rm cycle}$ as

$$t_{\rm cycle} \approx \frac{4}{c} \left(\frac{D_{\rm up}}{U_1} + \frac{D_{\rm dwn}}{U_2} \right) \sim \frac{D_{\rm up}}{cU} \tag{11}$$

for relativistic particles (Drury 1983), with U_1 and U_2 being defined in equation (1).

The rate of the energy gain of the particles is

$$\frac{\langle \Delta W \rangle}{dt} \sim \frac{U^2}{D_{\rm up}} W \sim \frac{W}{t_{\rm acc}} \tag{12}$$

[from equation (4), with $dt = t_{\rm cycle}$ from equation (11), and by assuming relativistic particle velocities], which defines the acceleration time $t_{\rm acc} \sim D_{\rm up}/U^2$.

Finally, the energy distribution has been estimated to be

$$N(E) \propto E^{-(1+t_{\rm acc}/t_{\rm esc})}, \tag{13}$$

(see Jones 1994; Achterberg 2008), with the escape time $t_{\rm esc} = t_{\rm cycle}/P_{\rm esc} \sim [D_{\rm up}/cU]/[U/c] \sim D_{\rm up}/U^2 \sim t_{\rm acc}$ (see equation (5), and by using t_{cycle} as a characteristic time scale) and $t_{\rm acc}$ from equation (12).

3 THE NUMERICAL MODEL

We construct a 3D grid ($N \times N \times N$) with linear size L. The box is separated into two parts that we call downstream and upstream region, and which represent, respectively, the area behind and in front of the shock discontinuity that itself is located at the middle plane. The grid is randomly filled by $N_{\rm sc_{dwn}}$ scatterers downstream and $N_{\rm sc_{up}} = N_{\rm sc_{dwn}}/r$ scatterers upstream, where r is the compression ratio (see equation 1). We define $R_{\rm up/dwn} = N_{\rm sc_{up/dwn}}/[N^2 \times (N-1)/2]$ as the fraction of grid point which are scatterers. The mean-free path the particles travel between two scatterers is different on the two sides of the discontinuity (see Fig. 1b) and it can be determined as $\lambda_{\rm sc_{up/dwn}} = \ell/R_{\rm up/dwn}$, with $\ell = L/(N-1)$ the grid width. The time between two shock crossings is $\Delta t = t_{\rm cycl} = t_{\rm up} + t_{\rm dwn}$ with $t_{\rm up/dwn}$ the mean time particles stays in the upstream/downstream region. At time $t = 0$ the injected distribution $n(W, t = 0)$ is a Maxwellian with temperature T.

The scatterers can be either elastic or active. In the case the interaction of the particles with the scatterers is elastic, the scatterers only affect the direction particles move after their interaction with the scatterer. When the scatterers are active a particle loses or gains energy in its interaction with the scatterers. Energization of the particles occurs in any case when the particles are crossing the shock wave. In Fig. 1(a) we show a small version (for better visualization) of the box with the downstream scatterers in blue and the upstream scatterers in red. The two upstream and downstream boundary planes of the box that are parallel to the shock surface are always open, and the four boundary planes that are perpendicular to the shock surface can be periodic (partially open box) or open (open box). The particles have a higher probability to escape from the downstream region than from the upstream region. We choose the initial position of the particles randomly and only in the upstream region, and everywhere the particles are bound to follow the grid-lines in their motion. The direction particles' move when they are upstream is randomly chosen only between five directions: the four directions parallel to the shock and the opposite direction to the shock normal, i.e. towards the shock front. A particle can escape from the upstream region e.g. when it moves from downstream to upstream and never meets a scatterer upstream, yet the probability for this to happen is very small. On the other hand, when particles are downstream, all directions of motion are equally probable when a particle encounters a scatterer. A typical trajectory of a particle inside the simulation box is shown in Fig. 1(b).

The parameters used in our simulations are related to the plasma parameters in the upper corona. We choose the magnetic field to be $B = 10$ G, the density of the plasma $n_0 = 10^7\ cm^{-3}$, the ambient temperature around 100 eV, the length L of the simulation box is 10^{10} cm, $R_{\rm dwn} = 10$ per cent, and we use $N = 601$ grid points in each direction. The Alfvén speed is comparable with the thermal speed of electrons ($V_{\rm A} \approx 7 \times 10^8$ cms^{-1}). The mean-free path of the particles upstream is $\lambda_{\rm sc_{up}} = L/[(N-1)R_{\rm up}] \sim 10^9$cm. The shock wave velocity is chosen as $U = M_{\rm A} \cdot V_{\rm A}$ with the Alfvén Mach number $M_{\rm A} = 5$. Each shock crossing changes the energy of the particles according to equation (3). Then, for relativistic particles ($\geq$1 MeV), the typical energy increment is of the order of $(\Delta W/W) \approx U/c \sim 10^{-1}$ for one round trip across the shock.

4 RESULTS

4.1 Elastic scattering

In this section we assume that the scatterers affect only the direction along which the particles travel inside the simulation box, and the box is partially open, only the upstream and downstream boundary of the box are open. The temporal evolution of the kinetic energy of typical electrons is presented in Fig. 1(c). The particles system-

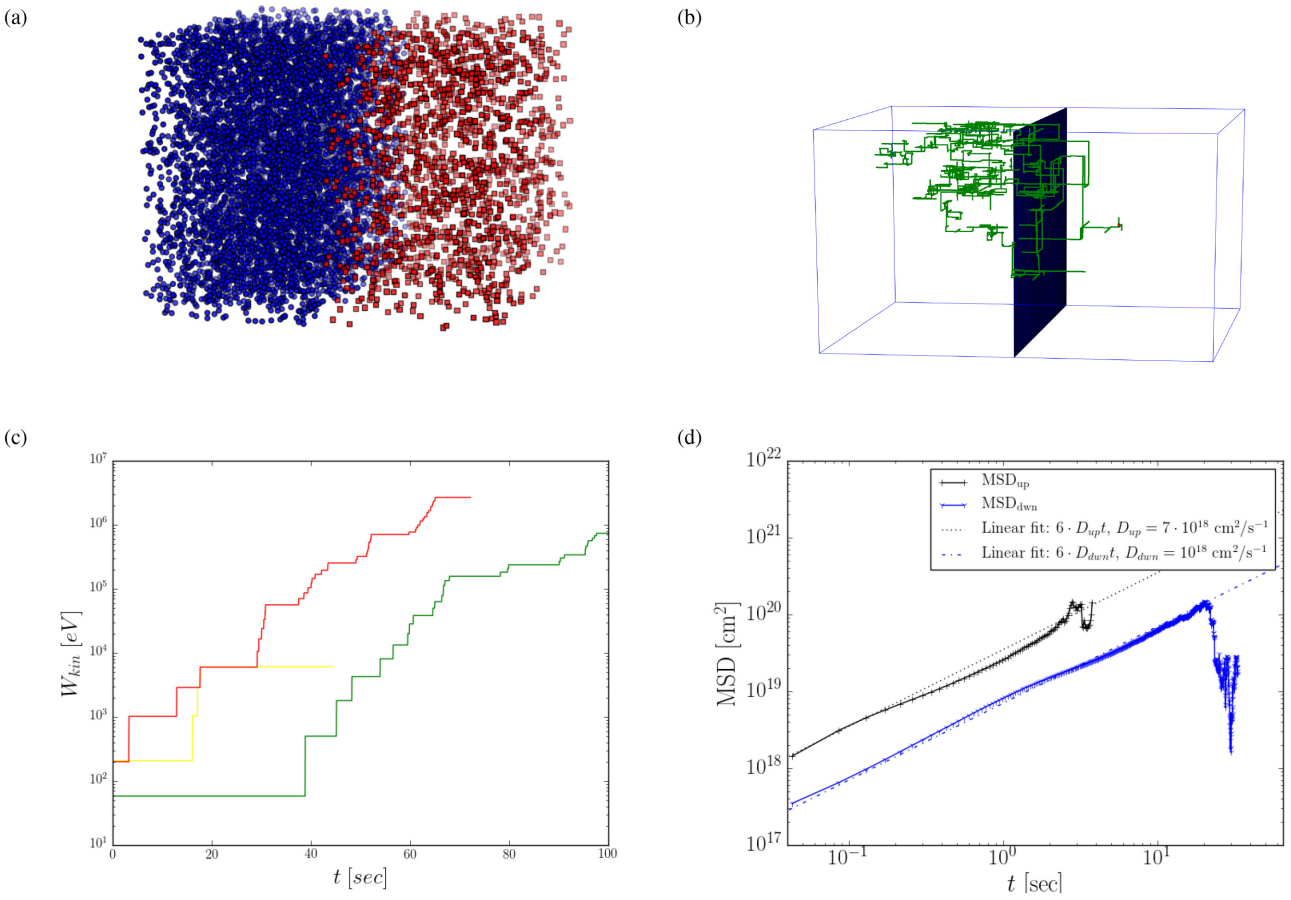

Figure 1. (a) Small version of the simulation box with the planar shock wave in the middle.(b) Trajectory of a typical electron inside the simulation box. (c) The kinetic energy increase of typical electrons travelling inside the simulation box as a function of time. Electrons gain systematically energy as they cross the shock. (d) Mean square displacement of the electrons upstream (black) and downstream (blue).

atically gain energy, which though happens only when they cross the shock discontinuity.

Our aim here is to compare our numerical results with the theoretical arguments and results presented in Section 2, so we use relativistic particles for our approximate estimates. It is important to stress that the relativistic particles appear in our simulations around 20 s after the injection of the thermal particles.

In Fig. 1(d) we show the mean square displacement of the particles $<R^2>$ as a function of time downstream and upstream. The diffusion of the particle is normal, as we would expect it for a random walk process, and a linear fit gives the estimates of the diffusion coefficients $D_{\rm up} \approx 8 \times 10^{18}{\rm cm}^2{\rm s}^{-1}$ and $D_{\rm dwn} \approx 10^{18}{\rm cm}^2{\rm s}^{-1}$. The value of $\lambda_{{\rm sc}_{\rm up}} \approx D_{\rm up}/U \sim 10^9{\rm cm}$, as yielded by equation (10), is thus in good agreement with the value that follows from the characteristics of our simulation set-up (see Section 3).

The average energy gain ratio for particles in one complete cycle around the shock surface is estimated from our simulation as $<\Delta W>/W \approx 0.1$, which is close to the theoretically expected value U/c [see equation (4) for the relativistic case].

From equations (6) and (7) we can estimate the time the particles spend upstream and downstream before they cross the discontinuity, $t_{{\rm up}_{\rm th}}, t_{{\rm dwn}_{\rm th}} \approx 0.26\,{\rm s}$, and comparing this with the values estimated from our simulation, we find $t_{{\rm up}_{\rm num}} \approx 0.19\,{\rm s}$ and $t_{{\rm dwn}_{\rm num}} \approx 0.39\,{\rm s}$. A typical particle completes a cycle around the shock discontinuity in $t_{{\rm cycl}_{\rm num}} \approx 0.58\,{\rm s}$, while when using the mean-free path or the diffusion coefficients [equations (8) and (11)] we estimate $t_{{\rm cycle}_{\rm th}} \approx 0.46\,{\rm s}$. All the values from test particle approximation are thus in close agreement with the theoretical results in Section 2.

We can also compare the estimate of $P_{\rm esc}$ from our model with the one predicted by the theory (see equation 5). We notice that the escape probability is energy independent, so for the estimate of $P_{\rm esc}$, it is relevant to take the median value of t_{cycle} of all particles and not just the relativistic ones. In this case we find $t_{\rm cycle} \approx 6.6\,{\rm s}$, and using the relation $P_{\rm esc} = t_{\rm cycle}/t_{\rm esc}$ (Achterberg 2008) we have $P_{\rm esc} \approx 0.15\,{\rm s}$, close to the theoretical value ($\approx$0.11).

The energy distribution of the electrons that have escaped after 150 s is presented in Fig. 2(a). We find that the energy distribution of the non-relativistic particles can be fitted with a Maxwelian distribution, and the high-energy tail with a power law with an index -2, as it is well known from theoretical arguments given in the literature and reported briefly in Section 2. (Concerning the different slopes of the two Maxwellian distributions in Fig. 2(a) at low energies, we note that the initial velocity is generated obeying a 3D Maxwellian, the particle motion though is bound to the grid so the final distribution follows a 1D Maxwellian.)

The temporal evolution of the mean kinetic energy is shown in Fig. 2(b). As we expect from equation (12), the energy increases exponentially after an initial transient period. We can estimate the acceleration time from the simulation through an exponential fit, which yields $t_{{\rm acc}_{\rm num}} \approx 28\,{\rm s}$, almost an order of magnitude slower than the estimated theoretical value $t_{\rm acc} \sim D_{\rm dwn}/U_2^2 \sim 2\,{\rm s}$ (see equation 12). This is probably related with the fact that all the

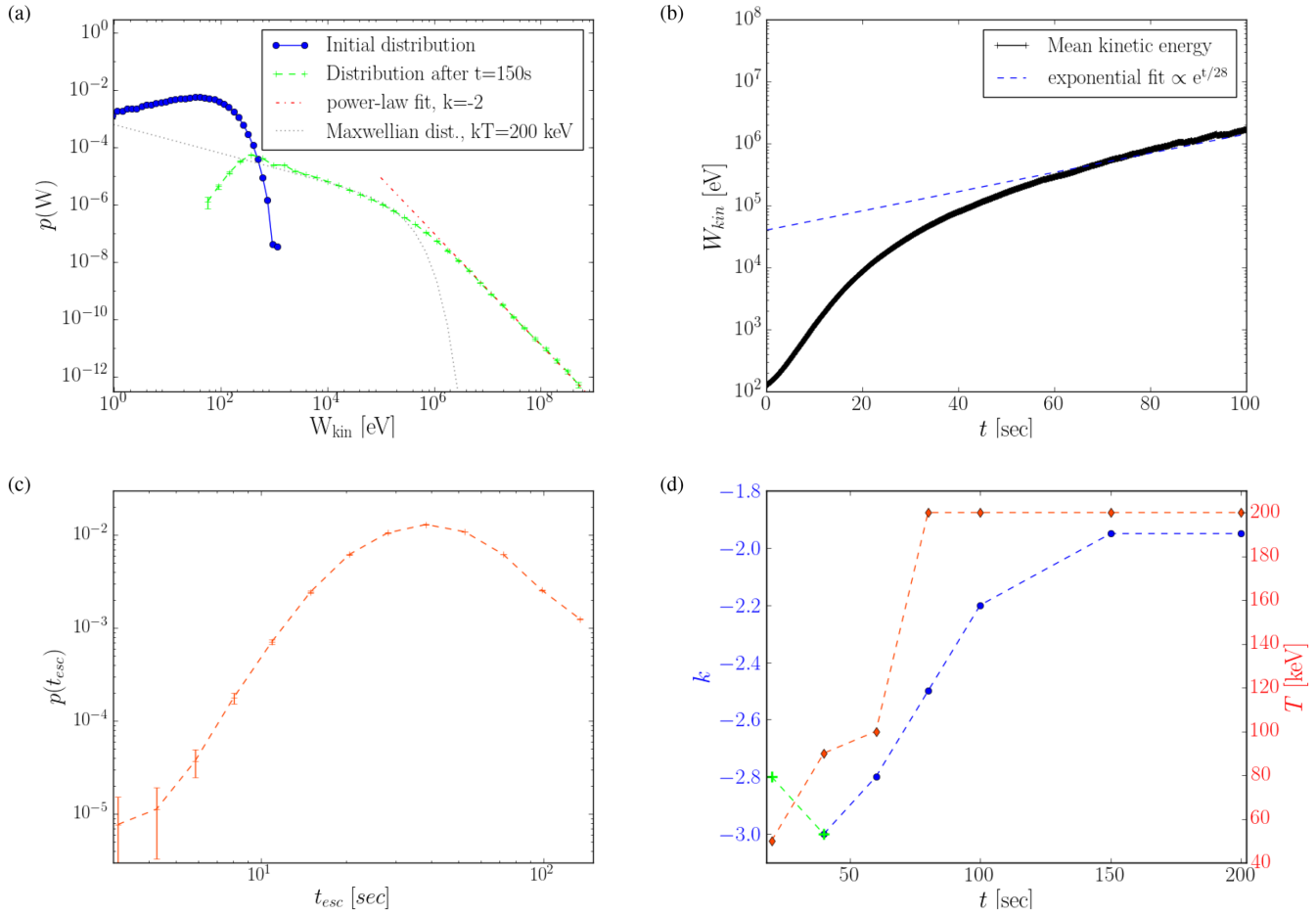

Figure 2. (a) The asymptotic kinetic energy distribution of the electrons escaping from the box downstream: initial energy distribution (blue), particles that have escaped from the box (green), together with a power-law fit W^k with $k = -2$ (red). (b) The evolution of the mean energy as a function of time (black) with an exponential fit (blue). (c) Distribution of the escape times of the electrons. (d) Parameters of the evolution of the energy distribution of electrons escaping downstream: The evolution of the power-law index of the relativistic electrons (blue; the green colour is for the power-law tail before particles have become relativistic), and the evolution of the temperature of the non-relativistic electrons (red).

particles, including the thermal ones, were taken into account for the numerical estimate, whereas the theoretical estimate was derived by making the assumption that all particles have relativistic energies. The mean t_{esc} is estimated to be ∼42 s.

Following the time evolution of the energy distribution of the escaping particles we can estimate the evolution of the temperature of the non-relativistic particles and the power-law index of the relativistic particles (see Fig. 2d). The energy distribution reaches its asymptotic shape approximately 100-150 s after the injection of the initial Maxwellian distribution with temperature ≈100 eV. The escaping distribution attains a temperature of around 200 KeV, and the high-energy tail has a power-law index −2 and extends to the maximum energy of ∼1 GeV, for the electrons considered here. Keeping all other physical parameters fixed (plasma density, magnetic field strength, Mach number, etc.), the crucial parameter that affects most of the estimates reported here is the scattering mean-free path, i.e. the density of the large-scale magnetic disturbances that scatter the particles. As we can see from equation (10), the diffusion coefficient is directly influenced by the scattering mean-free path, which will affect the acceleration time. This result has been confirmed by our simulations.

Most of the theoretical estimates reported in Section 2 are independent of the particle mass, so the acceleration time, the diffusion coefficients, the mean-free path, etc. are similar for the ions and the electrons and as estimated above. The energy distribution of the ions escaping downstream has the same characteristics with the energy distribution of the electrons (see Fig. 3). The energy distribution is again a Maxwellian distribution with a power-law tail with index $k \approx -2$. The difference between the energy distribution of the ions and the electrons is that the ions are hotter ($T \approx 200$ MeV) than the electrons downstream, and their power-law tail reaches higher energies (∼1000 GeV).

So far the simulation box used was partially open. For an open simulation box we again numerically estimate the diffusion coefficients, and we find them to remain unchanged, therefore t_{cycle} also stays the same (≈0.6 s). The main differences with the partially open box are the mean escape time and the acceleration time. Electrons barely reach relativistic energies (particles never exceed 1 MeV) and the energy distribution of particles escaping from the simulation box reaches an asymptotic state after around 40 s. The energy distribution shows moderate heating at the low energies and then forms a double power law, with index ≈− 1.3 at intermediate energies and index ≈− 4 at the high-energy tail (see Fig. 4). This distribution is similar to the energy distribution from the partially open box reached after 40 s, as one can see from Fig. 2(d). In other words, the electrons escape from the open simulation box

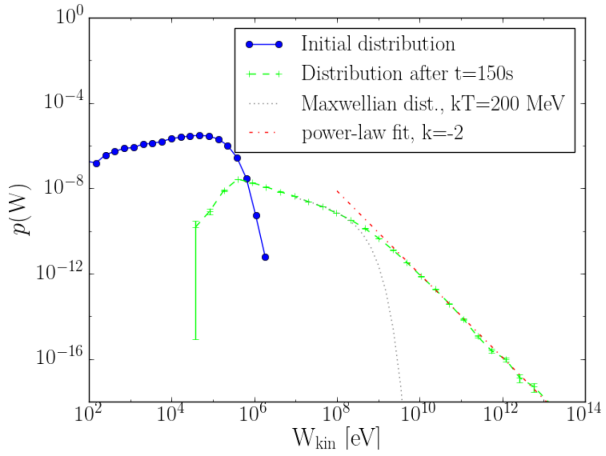

Figure 3. Energy distribution of the ions escaping from the partially open simulation box after reaching their asymptotic state (∼150 s) (green) and initial energy distribution (blue). The asymptotic energy distribution is a mixture of hot plasma with temperature T= 200 MeV (grey) with a power-law distribution with index $k = -2$ (red).

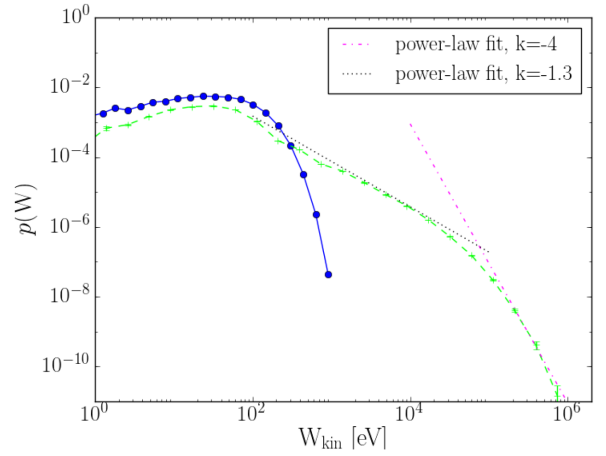

Figure 4. Initial energy distribution (blue) and the energy distribution of the electrons escaping from the box after 40 s (green), with two power-law fits $\propto W^k$ with $k = -1.3$ (black) and k= -4 (red), in an open simulation box, for the case of DSA.

before attaining to the asymptotic state reached in the partially open box.

In the case of ions in the open box, we obtain the same shape of the energy distribution as for the electrons (a Maxwellian at the low energies and a double power law at the high energies), yet the ions become hotter ($T \approx 30$ MeV), the double power-law tail is similar to the one of the electrons, and the maximum energy the ions reach is ∼1 GeV. In order with the open simulation box to get results similar to the ones from the partially open box, we would have to increase the trapping of the particles in the box by reducing the mean-free path of their interaction with the scatterers.

Our main finding so far is that the accelerated electrons and ions have the same shape of the energy distribution, namely a mixture of hot plasma with a power-law distribution at the high-energy tail. In order for the power-law tail to assume the well-known asymptotic index (−2), the particles must reach relativistic energies.

The numerical estimates and the analysis reported here are in good agreement with the well-known theoretical estimates for the DSA reported in the literature (see Section 2). In the next paragraph we use the same environment as above, with the only difference that the scatterers are considered to be active. We assume that large-amplitude magnetic fluctuations in the vicinity of the shock interact stochastically with the electrons and ions, as it was proposed and analysed initially by Fermi (Fermi 1949).

4.2 The role of stochastic Fermi energization for diffusive shock acceleration

The fact that high-amplitude magnetic fluctuations are present in the vicinity of a shock implies that they may also contribute substantially as scatterers to the acceleration of electrons and ions. These large-amplitude magnetic fluctuations are not waves, and their interaction with particles does not obey the quasi-linear wave-particle approximations. For the analysis of the interaction of electrons and ions with magnetic disturbances with $\delta B/B \geq 1$, we return to the analysis done initially by Fermi (see Parker & Tidman 1958; Ramaty 1979; Miller & Ramaty 1992; Pisokas et al. 2017).

The stochastic energy gain or loss of particles interacting with the scatterers upstream and downstream is

$$\frac{\Delta W}{W} \approx \frac{2}{c^2}\left(U_{1/2}^2 - \mathbf{U}_{1/2}\cdot\mathbf{v}\right), \tag{14}$$

where U_1 and U_2 is the velocity of the flow, respectively, upstream and downstream. The initial distribution of the particles is again a Maxwellian with temperature 100 eV (the ambient temperature of the plasma). At $t = 0$, all particles are located upstream at random positions on the grid and the initial direction of their motion follows the same rules as in the DSA model with the elastic scatterers discussed above in Section 4.1. As the grid constrains the motion of the particle, the term $\boldsymbol{U}_{1/2}\cdot\boldsymbol{v}$ has a sign randomly chosen among three possible values: –1 for head-on scatterings, 1 for overtaking scatterings, and 0 for perpendicular scatterings. The typical energy increment is then of the order of $(\Delta W/W) \approx (U_{1/2}/c)^2 \sim 10^{-3}$, so the energy gain is smaller per scattering off a magnetic fluctuation than in an energization event at the shock, but the number of interactions is much higher.

The kinetic energy as a function of time for three typical electrons is shown in Fig. 5(a). The electrons gain or lose energy stochastically when they interact with the magnetic disturbances and they systematically gain energy when they cross the shock at the times marked with circles in Fig. 5(a).

In the asymptotic state, the kinetic energy distribution of the electrons escaping from the open simulation box is a mixture of hot plasma with $T \approx 200$ keV, and a power-law tail with index $k = -2$ (see Fig. 5b). We note that both T and k progressively increase until they reach their asymptotic value (see Fig. 5e). The simulation box is chosen open since in a partially open box SDA together with stochastic scatterers leads to an over-efficient energization, and we would have to lower the density of the scatterers. Since we preferred to keep the parameters as before in Section 4.1, we allow for faster escape from an open box, which reduces the energization to a reasonably efficient level.

The escape times t_{esc} and acceleration times t_{acc} are shown in Figs 5(c) and (d). The acceleration time is estimated by fitting the mean kinetic energy as a function of time with an exponential (see Fig. 5c), which yields $t_{acc} \approx 2$ s that is an order of magnitude faster than in the pure DSA reported above. We note that the median escape time ($t_{esc} \approx 2.5$ s) is also an order of magnitude smaller than in the case of pure DSA. The synergy of stochastic acceleration by large-amplitude magnetic fluctuations and of systematic acceleration at

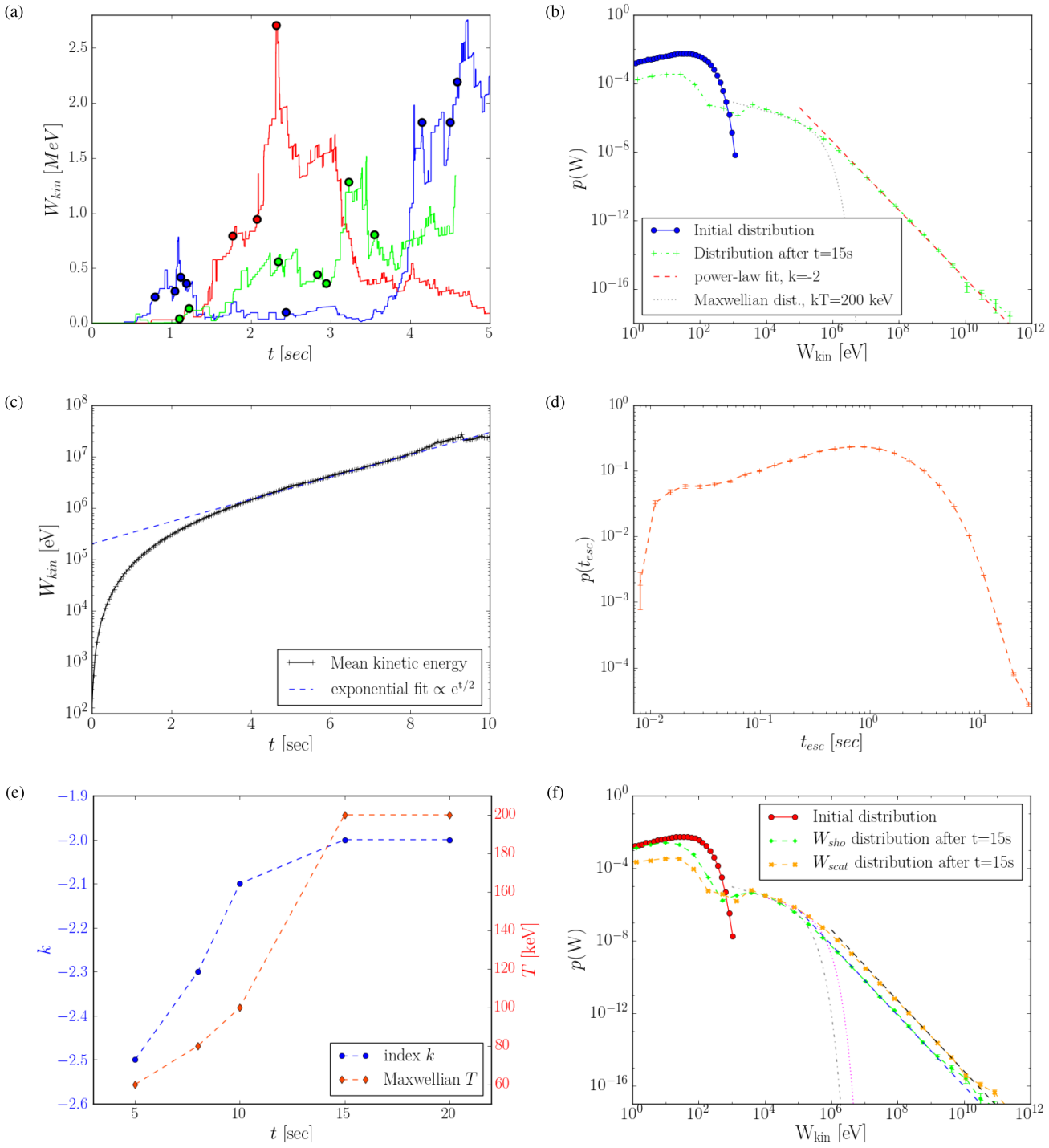

Figure 5. Characteristics of DSA in combination with stochastic interaction of electrons with magnetic disturbances: (a) Kinetic energy as a function of time for three typical particles, the circles mark shock crossings. (b) Initial kinetic energy distribution (blue) and kinetic energy distribution after 15 s for particles escaping from the box (green), with a power-law fit ($=W^{-2}$ (red)), and a Maxwellian distribution with temperature $T = 200$ keV (grey). (c) Mean kinetic energy as a function of time (black) with an exponential fit with slope ≈2 s (blue). (d) Distribution of the escape times t_{esc}. (e) Evolution of the index k of the power-law tail and of the temperature T of the Maxwellian fit. (f) Initial kinetic energy distribution (red), together with the kinetic energy distribution from the shock contribution only (green) and from the scattering contribution only (orange), together with power-law fits with indexes $k = -2$ (blue and black), and Maxwellian distributions with temperature T= 80 keV (grey) and $T = 200$ keV (pink).

the shock influences the efficiency of the electrons' acceleration and increases the maximum energy they reach by two orders of magnitude (≈100 GeV).

We keep track separately of the energy particles gain along their path from the scatterers ($W_{\rm scat}$) and from their crossings of the shock surface ($W_{\rm shock}$, the classical DSA result). Indeed, the distribution

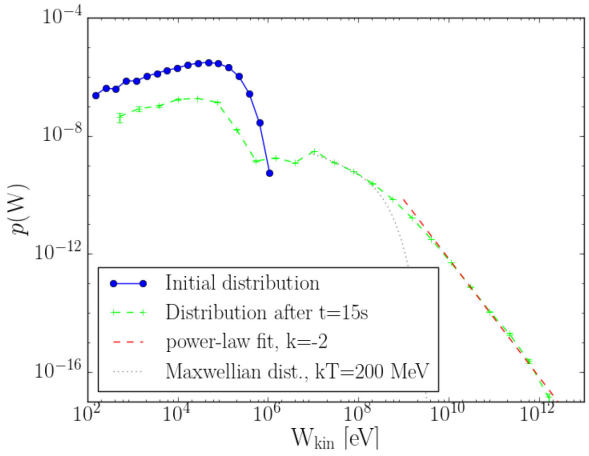

Figure 6. Ions in an environment of DSA combined with stochastic acceleration: Initial distribution (blue) and distribution of the ions escaping from the box (green) after 15 s, with a power-law fit $\propto W^k$ with $k = -2$ (red), and a Maxwelian distribution with temperature T= 200 GeV (grey).

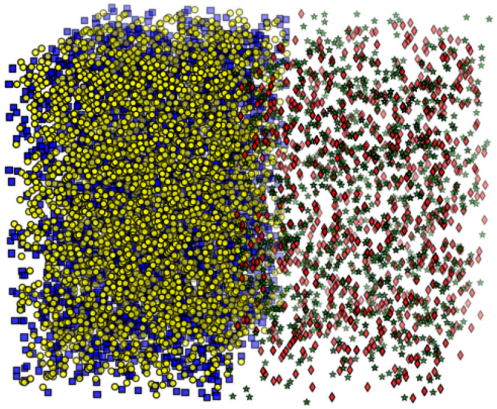

Figure 7. Small version of the box, with the stochastic scatterers upstream marked in red and downstream marked in blue. The randomly placed current sheets are marked in green upstream and in yellow downstream. 10 per cent of the grid points are active downstream (of which 50 per cent are stochastic scatterers and 50 per cent current sheets) and 2.5 per cent upstream (of which 50 per cent are stochastic scatterers and 50 per cent current sheets).

of $W_{\rm scat}$ is a mixture of hot plasma with temperature $T \approx 200$ keV, which coincides with the low-energy part of the final total distribution, and a power-law tail with index $k \approx -2$. The distribution of $W_{\rm shock}$ has the same general form as the energy distribution due to the interaction of the particles with the magnetic fluctuations, but with a lower temperature $T \approx 80$ keV (see Fig. 5f). Also, the ratio of the mean integrated energy gain from the scatterers and the shock $\langle W^t_{\rm scat}\rangle / \langle W^t_{\rm shock}\rangle$ is ≈6.6, i.e. the contribution of $W_{\rm scat}$ is around seven times bigger than the contribution of $W_{\rm shock}$. So, the stochastic interaction between magnetic fluctuations and particles dominates their heating and is equally effective in the acceleration of the high-energy tail. At the same time it retains the standard DSA characteristics for the heated and the accelerated particles. In most hybrid, PIC and MHD(PIC) simulations (see e.g. Caprioli & Spitkovsky 2014a,b,c; van Marle et al. 2018) one of the main arguments given that the simulations were successful to reproduce the results expected from DSA is the fact that the power-law index of the high-energy tail is close to -2. The combined effect of stochastic and systematic acceleration reported here maintains this result and influences mainly the efficiency of the accelerator.

The fact that the DSA and stochastic acceleration by large-amplitude magnetic disturbances can be similar was already pointed out by Jones (1994). He compared separately the two mechanisms and concluded that 'DSA has no particular advantage over stochastic acceleration'. In our opinion the synergy of the two mechanisms analysed here is even more appealing and much more efficient, and, as mentioned, the characteristics of the energy distribution remain the same as in the DSA.

Ions in this mixed environment of stochastic acceleration and DSA in an open simulation box have approximately the same $t_{\rm esc}$ and $t_{\rm acc}$ as the electrons. The kinetic energy distribution in the case of ions is shown in Fig. 6; it exhibits the same hybrid form of a Maxwellian and a power-law tail with index $k \approx -2$. The difference with the electrons is that the temperature of the ions is higher, $T \approx 200$ MeV, and the power-law tail reaches a higher maximum energy in the asymptotic state. $W_{\rm shock}$ and $W_{\rm scat}$ have the same relative contribution as previously reported for the electrons, so again the scattering process dominates. In the case of ions, the ratio $\langle W_{\rm scat}\rangle/\langle W_{\rm shock}\rangle$ is ≈5, so it is slightly lower than in the case of electrons. The distribution of W_{scat} is still a synthesis of hot plasma, but now with temperature $T \approx 200$ MeV, which again coincides with the low-energy part of the final total distribution, and a power-law tail with index $k \approx -2$, while $W_{\rm shock}$ has the same general form but with a temperature $T \approx 80$ MeV in the Maxwellian low-energy part.

4.3 Diffusive shock acceleration in the presence of turbulent reconnection

The presence of large-amplitude MHD disturbances, which is necessary to enhance the trapping of the charged particles in the vicinity of the shock, will spontaneously drive the TR state, as it is well documented in the literature reported in the Introduction.

Pisokas et al. (2018) analysed the synergy of stochastic and systematic acceleration that takes place when an unstable plasma reaches the state of TR. In this article, we expand many of the concepts developed by Pisokas et al. (2018) in order to couple the Diffusive Shock Accelerator with Turbulent Acceleration in the vicinity of a shock.

We keep the same basic configuration for the simulation box, changing though the properties of the active grid points. Now the scatterers are divided into two classes, a fraction P are stochastic scatterers, exactly as the ones considered in the previous subsection, and the rest $(1 - P)$ are UCSs (see Pisokas et al. 2018). For the rest of this section we choose P= 0.5; the environment we consider is illustrated in Fig. 7. The injected particles have the same initial distribution as before. When a particle meets a large-amplitude magnetic disturbance, its energy changes according to equation (14), as before. For UCSs as scatterers, the energy gain is caused by electric fields and it follows the relation

$$\Delta W = \mid e \mid E_{\rm eff} \ell_{\rm eff}, \tag{15}$$

with e the charge of a particle, and $E_{\rm eff} \approx (U_{1/2}/c)\,\delta B$ is a measure of the effective electric field of the UCS (Kowal, de Gouveia Dal Pino & Lazarian 2011). U_1 and U_2 are the velocity of the flow upstream and downstream, respectively, and δB is the fluctuating magnetic field. Reconnection at an UCS induces stochastic fluctuations, so δB is of stochastic nature, and we assume that it obeys a power-law distribution with index 5/3 in the range $[10^{-5}G; 100G]$, i.e. it follows a Kolmogorov spectrum. Finally, the effective length $\ell_{\rm eff}$ is assumed as an increasing linear function of $E_{\rm eff}$, restricted to values between

10 m and 1 km. We note that the interaction between particles and UCSs always leads to a positive energy increment (systematic energy gain), which also is not dependent on the instantaneous energy of the particles.

The synergy of large-scale magnetic disturbances with randomly distributed UCS, studied in Pisokas et al. (2018), is now investigated in the presence of an additional systematic accelerator, the DSA.

Fig. 8(a) shows the time evolution of the kinetic energy of a few typical particles. The picture here is similar to the case of DSA together with stochastic scatterers (Fig. 5a); there is a random walk like behaviour with an increasing trend, the latter being though more pronounced in the presence of UCSs that are also systematic accelerators.

The energy distribution of the electrons escaping from the simulation box after reaching the asymptotic state is again a synthesis of a hot plasma with temperature ≈100 keV and a high-energy power-law tail with index $k \approx -2$ (see Fig. 8b). The maximum energy particles reach is ≈10 GeV, so it is comparable with the case we discussed before where UCS were absent ($P = 1$). We note that at times before t= 15 s, there actually is a double power law, one at intermediate energies and one at the high-energy tail, which at about t= 15 s merge and attain to the same index −2 (see Fig. 8e). The appearance of this double power law must be attributed to the presence of the UCSs. The UCSs' effect is thus of equal importance than the one of the DSA and the stochastic scatterers, mainly though at early times, before the asymptotic state is being reached. That the action of the UCSs is limited to early times can be explained by the fact that in their case the energy increments do not depend on the energy of the particles, so they are most efficient in the phase where particles still have relatively low energies, and at later times the more energetic particles are accelerated mostly by the systematic acceleration of the DSA and by the stochastic acceleration through the large-amplitude magnetic disturbances.

The median value of the escape times is $t_{esc} \approx 3.7$ s (see Fig. 8c), so it is about 1 s more than in the case of $P = 1$. This result is in agreement with the result reported by Pisokas et al. (2018) on the role played by the UCS in the trapping of particles inside a Turbulently Reconnecting volume. The acceleration time is increased compared to the $P = 1$ case, we find $t_{acc} \approx 4.5$ s (see Fig. 8d).

Keeping track of the source of each energy gain from one of the three acceleration processes (stochastic acceleration by large-scale magnetic disturbances, acceleration at UCS and DSA) along the trajectories of the particles, we can analyse the contribution of each accelerator separately. Fig. 8(f) shows the kinetic energy distribution due to each acceleration process separately. In all cases there are power-law tails, with the DSA and the stochastic scatterers exhibiting the same index −2, and the power law due to the UCSs being flatter with index −1.4 at the intermediate energies and index −1.8 at the high energies. This again confirms that at large times the role of the UCSs is limited.

It is important to note that the synergy of the UCS and the DSA (the case $P = 0$) has been studied by several authors (see Zank et al. 2015; le Roux et al. 2016), who pointed out that the energy distribution of the accelerated particles is harder (∼1.8) in this case. As we already mentioned, this result also appears in our simulation at times before the energy distribution reaches an asymptotic state (see Fig. 8e at about t= 5 s). Our study thus lets us conclude that the index 1.8 found by Zank et al. (2015) and le Roux et al. (2016) is the result of the action of UCSs, and not of DSA.

The asymptotic energy distribution of the ions is slightly different from the one of the electrons, the power-law tail index is now $k \approx -2.2$, coinciding with the one following from the relation $k = -(1 + t_{acc}/t_{esc})$, with the same t_{acc} (≈4.5 s) as for $P = 1$ (DSA together with stochastic scatterers) and also almost the same t_{esc} (≈3.8 s), and thus, with the prediction of equation (13) being fulfilled, we can say that stochastic acceleration together with DSA dominates the energization of the ions. Also, the ions reach a higher maximal energy (≈1000 GeV), and from a Maxwellian fit to the low-energy particles' distribution we recover the fact that ions are hotter than electrons ($T \approx 200$ MeV).

5 DISCUSSION AND SUMMARY

In this article we simulate a large-scale shock in the upper solar corona, formed e.g. by a CME, till the energy distributions of electrons and ions reach their asymptotic state. We use as many pieces of information as possible from the microscopic analysis of current numerical simulations, but our emphasis here is on realistic spatial and temporal scales. We move progressively from elastic scatterers to active scatterers (stochastic interaction with large-amplitude magnetic fluctuations and systematic scattering at UCSs) in the vicinity of the shock, and our main results are as follows:

(i) We have analysed three distinct accelerators (1) DSA with passive scatterers, (2) DSA with stochastic scatterers and (3) DSA with TR (a combination of stochastic scatterers, as before, and UCSs). The asymptotic energy distribution of the particles escaping from the simulation box remains the same in all numerical experiments, a mixture of a hot plasma with a power-law tail with index -2 for the high-energy particles.

(ii) The presence of active scatterers in the vicinity of the shock does not affect the universal form of the energy distribution, only the acceleration time becomes shorter and the maximum energy reached by the high-energy particles increases by one or two orders of magnitude.

(iii) Keeping track of the source of the energy gain along the particles' trajectories, we have shown that the active scatterers contribute five to six times more energy than the DSA, and the energy distribution of the particles retains the main characteristics we have found in the case of DSA with passive scatterers.

(iv) The synergy of DSA and UCSs gives the same mixture of a hot plasma and a power-law tail, yet with harder power-law index ($k \sim 1.8$) at early times, as it had been pointed out already in the literature (see Zank et al. 2015; le Roux et al. 2016).

(v) The appearance of a power-law tail with index -2 often is considered to be characteristic for DSA; we though stress here that this result has been found for TR alone, in the absence of a shock (see Pisokas et al. 2018). TR thus gives results very similar with the ones of the synergy of DSA and TR.

(vi) The ions acquire the same shape of the energy distribution as the electrons, yet their energy gain is on slower scales, the maximum energy reached is higher than for the electrons, and the temperature of the low-energy particles is higher than the one of the electrons.

In our opinion, at a travelling shock (e.g. during a CME) initially DSA may dominate the heating and acceleration of particles, soon though the synergy of DSA and TR will become the main acceleration mechanism. In the final stages, when the non-linear phenomena have become very strong and the shock has been fragmented, TR continues as a moving sheath around the shock surface. The remarkable result from our study is that in all these stages of the shock evolution the accelerated particles have a universal energy distribution in the asymptotic state, namely a synthesis of a Maxwellian for the low-energy particles with a power-law tail with constant index for the high-energy particles.

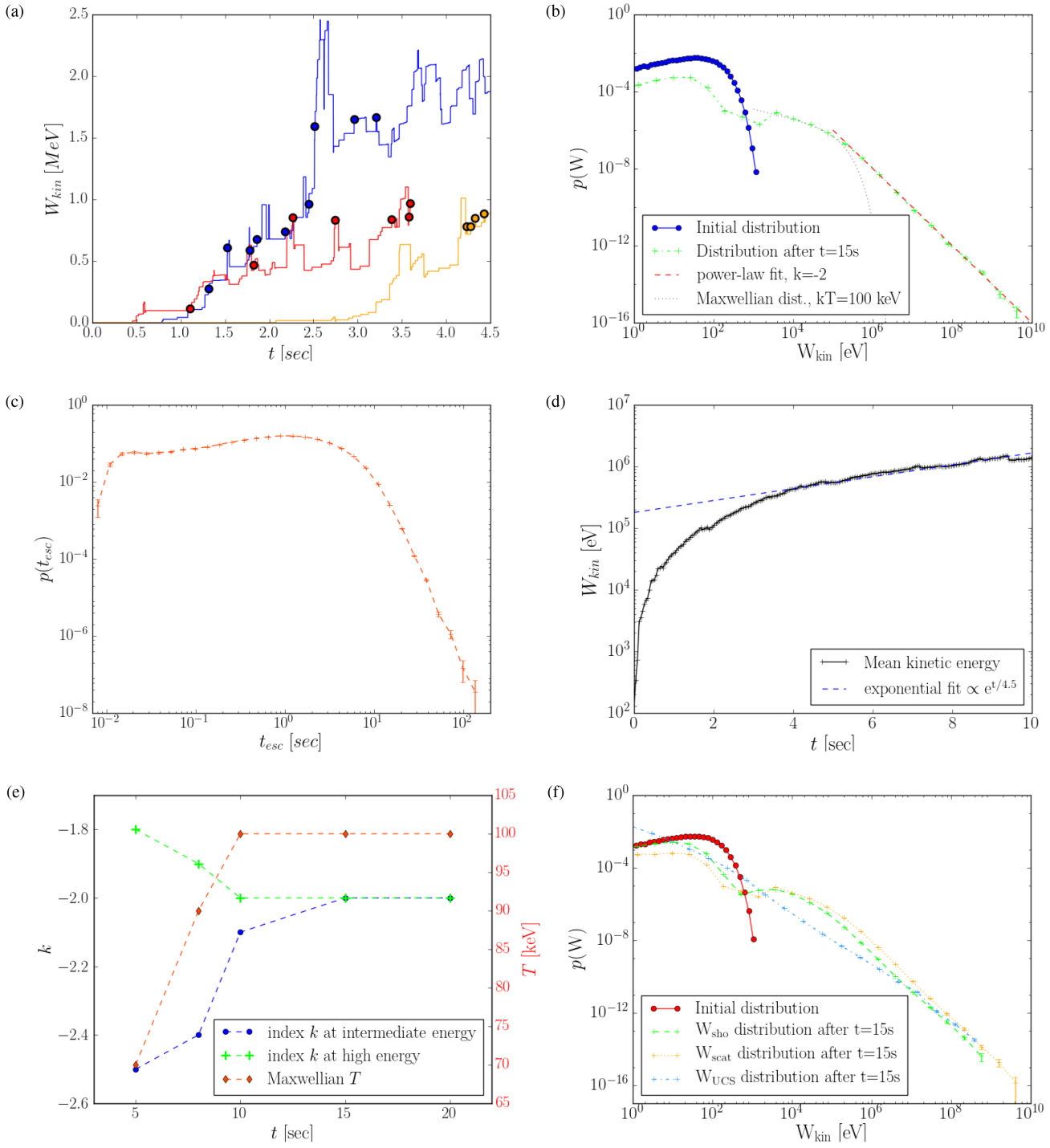

Figure 8. Acceleration of electrons by the synergy of TR and DSA: (a) The kinetic energy evolution of typical electrons interacting with the three accelerators. The circles mark the crossings of the shock surface. (b) Initial kinetic energy distribution (blue) and distribution after 15 s for electrons escaping from the box (green), with a power-law fit ($=W^{-2}$ (red)) and a Maxwellian distribution with temperature T= 100 keV (grey). (c) Distribution of the escape times t_{esc}. (d) Mean kinetic energy as a function of time (black), with an exponential fit (blue). (e) Evolution of the index k of the power-law tail at high energies (green), and of the power-law index at intermediate energies (blue), together with the evolution of the temperature T of the Maxwellian fit (red). (f) Initial kinetic energy distribution (red), the distribution from the shock contribution only (green), from the stochastic scatterers contribution only (orange) and from the UCSs contribution only (blue).

ACKNOWLEDGEMENTS

CG thanks the Observatoire de la *Côte d'Azur*, the University of Thessaloniki and the Erasmus$^+$ programme for making this joint research work possible. LV and HI thank the national Programme for the Controlled Thermonuclear Fusion, Hellenic Republic for their financial support. The sponsors do not bear any responsibility for the content of this work.

REFERENCES

Achterberg A., 1981, A&A, 97, 259
Achterberg A., 2008, Cosmic Accelerators, Lecture Notes for the Inter-University Lectures Series
Ambrosiano J., Matthaeus W. H., Goldstein M. L., Plante D., 1988, J. Geophys. Res.: Space Phys., 93, 14383
Arzner K., Vlahos L., 2004, ApJ, 605, L69
Arzner K., Knaepen B., Carati D., Denewet N., Vlahos L., 2006, ApJ, 637, 322
Axford W. I., Leer E., Skadron G., 1978 , in Shaviv G., ed., Cosmophysics, p. 125
Bai X.-N., Caprioli D., Sironi L., Spitkovsky A., 2015, ApJ, 809, 55
Balsara D., Kim J., 2005, ApJ, 634, 390
Balsara D., Benjamin R., Cox D. P., 2001, ApJ, 563, 800
Bell A. R., 1978, MNRAS, 182, 147
Bell A. R., 2004, MNRAS, 353, 550
Biskamp D., Welter H., 1989, Phys. Fluids B, 1, 1964
Blandford R. D., Ostriker J. P., 1978, ApJ, 221, L29
Burgess D., Möbius E., Scholer M., 2012, Space Sci. Rev., 173, 5
Burgess D., Gingell P. W., Matteini L., 2016, ApJ, 822, 38
Bykov A. M., Brandenburg A., Malkov M. A., Osipov S. M., 2013, Space Sci. Rev., 178, 201
Caprioli D., Spitkovsky A., 2014a, ApJ, 783, 91
Caprioli D., Spitkovsky A., 2014b, ApJ, 794, 46
Caprioli D., Spitkovsky A., 2014c, ApJ, 794, 47
Chasapis A. et al., 2015, ApJ, 804, L1
del Valle M. V., Lazarian A., Santos-Lima, R, , 2016, MNRAS, 458, 1645
Dmitruk P., Matthaeus W., Seenu N., Brown M. R., 2003, ApJ, 597, L81
Dmitruk P., Matthaeus W. H., Seenu N., 2004, ApJ, 617, 667
Drake J. F., Opher M., Swisdak M., Chamoun J. N., 2010, ApJ, 709, 963
Drury L. O., 1983, Rep. Progress Phys., 46, 973
Fermi E., 1949, Phys. Rev., 75, 1169
Fermi E., 1954, ApJ, 119, 1
Giacalone J., Jokipii J.R., 2018, ApJ, 663, L41
Isliker H., Vlahos L., Constantinescu D., 2017a, Phys. Rev. Lett., 119, 045101
Isliker H., Pisokas T., Vlahos L., Anastasiadis A., 2017b, ApJ, 849, 35
Jones F. C., 1994, ApJS, 90, 561
Karimabadi H., Lazarian A., 2013, Phys. Plasmas, 20, 112102
Karimabadi H., Roytershteyn V., Daughton W., Liu Y.-H., 2013, Space Sci. Rev., 178, 307
Karimabadi H. et al., 2014, Phys. Plasmas, 21, 062308
Khabarova O. V., Zank G. P., 2017, ApJ, 843, 4
Khabarova O. V., Zank G. P., Li G., Malandraki O. E., le Roux J. A., Webb G. M., 2016, ApJ, 827, 122
Kowal G., de Gouveia Dal Pino E. M., Lazarian A., 2011, ApJ, 735, 102
Krymskii G. F., 1977, Akademiia Nauk SSSR Doklady, 234, 1306
Kulsrud R. M., Ferrari A., 1971, Astrophys. Space Sci., 12, 302
Lazarian A., Opher M., 2009, ApJ, 703, 8
Lazarian A., Vishniac E. T., 1999, ApJ, 517, 700
Lazarian A., Eyink G., Vishniac E., Kowal G., 2015, Philosophical Trans. R. Soc. Lond. Ser. A, 373, 20140144
le Roux J. A., Zank G. P., Webb G. M., Khabarova O. V., 2016, ApJ, 827, 47
Longair M. S., 2011, High Energy Astrophysics. Cambridge University Press, Cambridge
Matsumoto Y., Amano T., Kato T. N., Hoshino M., 2015, Science, 347, 974
Matthaeus W. H., Lamkin S. L., 1986, Phys. Fluids, 29, 2513
Matthaeus W. H., Velli M., 2011, Space Sci. Rev., 160, 145
Matthaeus W. H., Wan M., Servidio S., Greco A., Osman K. T., Oughton S., Dmitruk P., 2015, Phil. Trans. R. Soc. A, 373, doi: 10.1098/rsta.2014.0154
Melrose D. B., 1994, ApJS, 90, 623
Melrose D. B., 2009, preprint (arXiv:0902.1803)
Miller J. A., Ramaty R., 1992, in Zank G. P., Gaisser T. K., eds, Particle Acceleration in Cosmic Plasmas, Am. Inst. Phys. Conf. Ser., New York, Vol. 264, p. 223
Miller J. A., Guessoum N., Ramaty R., 1990, ApJ, 361, 701
Miller J. A. et al., 1997, J. Geophys. Res., 102, 14631
Osman K. T., Matthaeus W. H., Gosling J. T., Greco A., Servidio S., Hnat B., Chapman S. C., Phan T. D., 2014, Phys. Rev. Lett., 112, 215002
Parker E. N., Tidman D. A., 1958, Phys. Rev., 111, 1206
Petrosian V., 2012, Space Sci. Rev., 173, 535
Pisokas T., Vlahos L., Isliker H., Tsiolis V., Anastasiadis A., 2017, ApJ, 835, 214
Pisokas T., Vlahos L., Isliker H., 2018, ApJ, 852, 64
Ramaty R., 1979, in Arons J., McKee C., Max C., eds, Particle Acceleration Mechanisms in Astrophysics, American Institute of Physics Conference Series, Vol. 56. p. 135
Schure K. M., Bell A. R., O'C Drury L., Bykov A. M., 2012, Space Sci. Rev., 173, 491
Servidio S., Matthaeus W. H., Shay M. A., Dmitruk P., Cassak P. A., Wan M., 2010, Phys. Plasmas, 17, 032315
Servidio S. et al., 2011, Nonlinear Process. Geophys., 18, 675
van Marle A. J., Casse F., Marcowith A., 2018, MNRAS, 473, 3394
Vlahos L., Pisokas T., Isliker H., Tsiolis V., Anastasiadis A., 2016, ApJ, 827, L3
Zank G. P., le Roux J. A., Webb G. M., Dosch A., Khabarova O., 2014, ApJ, 797, 28
Zank G. P. et al., 2015, ApJ, 814, 137

This paper has been typeset from a TEX/LATEX file prepared by the author.